JOC The Journal of Organic Chemistry

Article

pubs.acs.org/joc

Synthesis of N-substituted Pyrido[4,3-*d*]pyrimidines for the Large-Scale Production of Self-Assembled Rosettes and Nanotubes

Asuman Durmus,[†] Gorkem Gunbas,[†] Steven C. Farmer,[†] Marilyn M. Olmstead,[†] Mark Mascal,*[,†] Belete Legese,[‡] Jae-Young Cho,[‡] Rachel L. Beingessner,[‡] Takeshi Yamazaki,[‡] and Hicham Fenniri*[,‡,§,∥]

[†]Department of Chemistry, University of California Davis, 1 Shields Avenue, Davis, California 95616, United States

[‡]Department of Chemistry and National Institute for Nanotechnology, University of Alberta, 11421 Saskatchewan Drive, Edmonton, Alberta T6G 2M9, Canada

[§]Department of Chemical Engineering, Northeastern University, 360 Huntington Avenue, Boston Massachusetts 02115, United States

[∥]Qatar Biomedical Research Institute, Qatar Foundation, P.O. Box 5825, Doha, Qatar

Supporting Information

ABSTRACT: N-substituted pyrido[4,3-*d*]pyrimidines are heterocycles which exhibit the asymmetric hydrogen bonding codes of both guanine and cytosine at 60° angles to each other, such that the molecules self-organize unambiguously into a cyclic hexamer, assembled via 18 intermolecular hydrogen bonds. The synthesis is straightforward and can be concluded in six steps from the commercially available malononitrile dimer. X-ray crystallographic analysis of the supermacrocyclic structure shows an undulating disk with a ca. 10.5 Å cavity, the centers of which do not overlap sufficiently to describe a channel in the solid state. However, AFM, SEM, and TEM imaging in solution reveals the formation of 1D nanostructures in agreement with their self-assembly into rosette supermacrocycles, which then stack linearly to form rosette nanotubes.

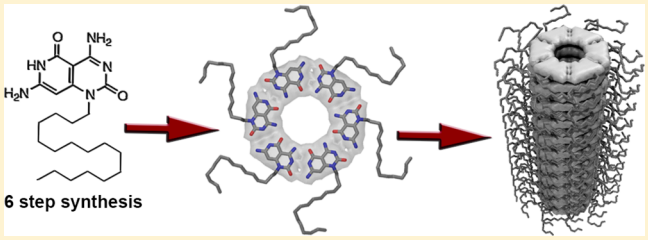

INTRODUCTION

The two principal branches of supramolecular chemistry, host–guest complexation and molecular self-assembly, have each yielded prodigious fruit in their respective spheres of science. While the former has provided a basis for multiple sequestering and sensing technologies, the latter has become largely associated with the burgeoning fields of crystal engineering and nanotechnology. In particular, materials that self-assemble into nanotubes have been the focus of intense activity, due to their potential to engage in selective (ionic, electronic, photonic) transport processes.[1]

Despite the ongoing interest in populating the supramolecular toolkit with new descriptions of noncovalent bonding, recent examples being anion–π interactions[2] and halogen bonding,[3] the hydrogen bond remains prominent in the design of both solution and solid-state self-organizing systems, due to its strength and directionality, witnessed by the extent to which it occurs in nature across a variety of functional and structural roles.

G∧C nucleobase hybrid **1** possesses the hydrogen-bonding faces of both guanine and cytosine at 60° angles to each other, defining an algorithm for the generation of hexagonal order on the supramolecular scale.[4,5] The presentation of reciprocal, asymmetric hydrogen-bonding codes (i.e., DDA-AAD, where A = H-bond acceptor, D = H-bond donor) permits no ambiguity in the recognition process and results in a highly robust ensemble of 18 intermolecular hydrogen bonds, with each base hybrid pairing contributing an association energy of 29.7 kcal mol^{-1}.[6] Recently, base hybrids with functional side chains (such as **2**), enabling the co-organization of virtually any species in the hexagonal periphery have been reported.[4,5,7] The synthesis of G∧C derivatives using nucleophilic aromatic substitutions, reductive amination, and cross-coupling chemistry have also been reported as a means to functionalize the resulting assemblies.[4,5,7]

Concurrent with these studies and continuing to the present time, several other cyclic, self-organized H-bonding systems have been described in the literature.[8] Interest remains high, for example, in the cyclic guanine quadruplex observed in nucleic acids[9] and two-dimensional patterning for the selective adsorption of guest entities onto surfaces.[10] But perhaps the most attractive opportunity presented by disk-shaped assemblies is to stack them, and if there is a void in the center of the disk large enough to accommodate a separate species, a nanotube is the result. While this behavior was previously demonstrated in the case of nucleobase hybrid rosettes,[4d,5b−d,11] the synthetic approaches to the subunits have generally involved considerable effort.[5c,d] Furthermore, despite the extensive characterization of aggregates of these species by a

Received: September 6, 2013
Published: October 16, 2013

   dx.doi.org/10.1021/jo4019792 | J. Org. Chem. 2013, 78, 11421−11426

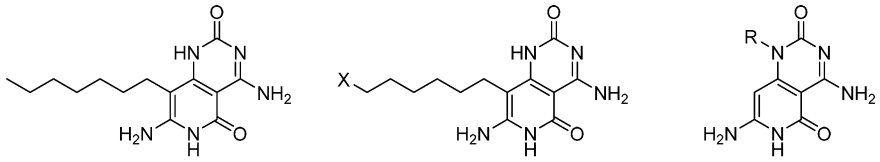

1 2a, X=Br 2b, X=OH 3

variety of spectroscopic and imaging techniques,[4d,5c,d,11] only a single solid-state structure of a DDA-AAD coded species ($\mathbf{1}_6$) has been reported to date.[4a] Here, we describe an efficient and short synthetic approach to the new hexamer-forming G∧C hybrid **3**, its X-ray crystal structure, and the imaging of the rosette nanotubes (RNTs) generated therefrom.

RESULTS AND DISCUSSION

A key design feature in our synthetic strategy resides in the placement of the side chain in target molecule **3**, which branches off the N-1 position of the cytosine ring. We reasoned that, by introducing the side chain in this position late in the synthesis, protection−deprotection schemes would be avoided in cases where the tail group terminates with a functional group, such as in **2**. Also, the redundant NH donor group in **1** is substituted in **3**, which renders the molecule less hydrophilic and less prone to pyridine−hydroxypyridine tautomerism, effectively locking the hydrogen-bonding array of the cytosine ring in the correct AAD configuration, regardless of the solvent type used for subsequent self-assembly.

A simple, six-step approach to **3** is shown in Scheme 1. Two derivatives were prepared, one with an *n*-heptyl chain (**3a**) for crystallization studies and one with a better solubilizing *n*-hexadecyl chain (**3b**) to facilitate nanotube formation in solution. Thus, the commercial malononitrile dimer **4** was cyclized in HBr/AcOH to the pyridine derivative **5**. Acetylation of **5** took place at the more nucleophilic amino group to give **6**, which permitted selective aminocarbonylation with trichloroacetyl isocyanate and subsequent base-induced ring closure with concurrent substitution of the bromo group to give **7**. Alkylation of **7** proceeds smoothly in DMF to give the nucleobase hybrid precursors **8**, which can be demethylated with *in situ* generated trimethylsilyl iodide to target compounds **3**.

Scheme 1[a]

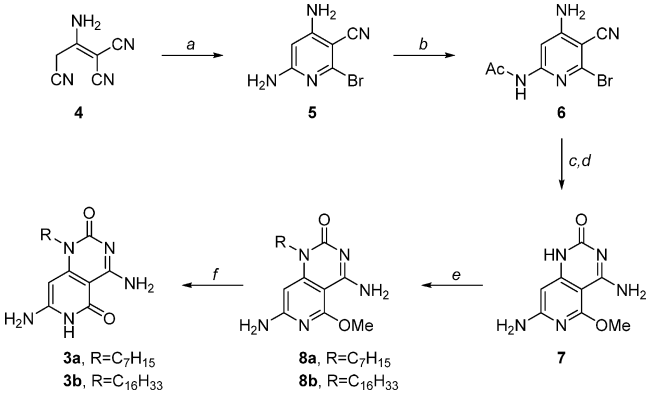

[a]Reagents and conditions: (*a*) 33% HBr−HOAc, 79%; (*b*) CH_3COCl, pyridine, 80%; (*c*) $Cl_3CCONCO$, CH_2Cl_2; (*d*) NaOMe, MeOH, 73% over two steps; (*e*) NaH, NaI, RBr, DMF, 75% (**8a**), 64% (**8b**); (*f*) TMSCl, NaI, MeCN, 76% (**3a**), 96% (**3b**).

We succeeded in crystallizing **3a** by heating a small sample in DMSO and cooling the solution slowly to room temperature.[12] The molecule crystallizes in the triclinic $P\bar{1}$ space group, with three independent molecules of **3a** in the asymmetric unit along with three molecules of dimethyl sulfoxide. Two such units related by inversion merge together to form the supermacrocyclic structure shown in Figure 1a. The hydrogen bonds between the six molecules of **3a** range from 2.768 Å (N···O) to 2.899 Å (N···N). In addition, the other NH_2 hydrogen is engaged in intramolecular hydrogen bonding to its neighboring carbonyl oxygen at an average N···O distance of 2.656 Å, giving a total of 24 hydrogen bonds per hexamer. Six DMSO molecules around the periphery and two in the interior of the hexamer contribute another eight hydrogen bonds to the overall structure. All three side chains differ conformationally, with one showing all *anti* relationships along the C_7 chain, the second showing one *gauche* conformation, and the third showing two *gauche* conformations. As shown in Figure 1b, the hexamer is not flat but undulating, with the maximum deviation from the mean plane defined by the 60 ring atoms being 0.480 Å (C5A) or, if the substituent atoms directly connected to the rings are included, 0.798 Å (N5A). The cavity enclosed by the six subunits, measured from opposing nitrogens or opposing oxygens, is between 10.4 and 10.6 Å across. The hexamers do not stack in a tubelike fashion in the solid state but rather as offset rings. A portion of this motif is shown in Figure 1c. The resulting void spaces accommodate the alkyl chains and also solvent molecules. Interestingly, this result is at variance with the only other crystal structure of a G∧C hexamer, i.e. that of **1**,[4a] in which case the hexamers overlapped with one another to describe channels that extended through the crystal. However, the units did not stack in the traditional sense but were separated by about 20 Å along the channel axis, unlike the case in **3b**, where the hexamers approach each other at stacking distances as close as 3.2 Å.

While crystals of **3a** from DMSO revealed the hexameric organization of the motifs in the solid state, the limited solubility of this material proved challenging for the self-assembly studies in solution. In contrast to **3a**, compound **3b** with the longer aliphatic *n*-hexadecyl side chain had good solubility in a variety of solvents at room temperature, notably cyclohexane (2.4×10^{-4} M). Time-dependent SEM, TEM, STEM, and AFM studies (Figure 2 a−e and Figures S1−S4 (Supporting Information)) showed that **3b** self-assembles into RNTs within 10 min. The average diameter of single RNTs measured by TM-AFM was 3.8 ± 0.3 nm. This is lower than the TEM measurement of 4.8 ± 0.3 nm and the predicted value of 4.4 nm (Figure S7 (Supporting Information)), as a result of the tip-induced compression of the nanotubes.[13]

The self-assembly of **3b** (2.4×10^{-5} M) was also studied using UV−visible spectroscopy. As shown in the time-

dx.doi.org/10.1021/jo4019792 | J. Org. Chem. 2013, 78, 11421−11426

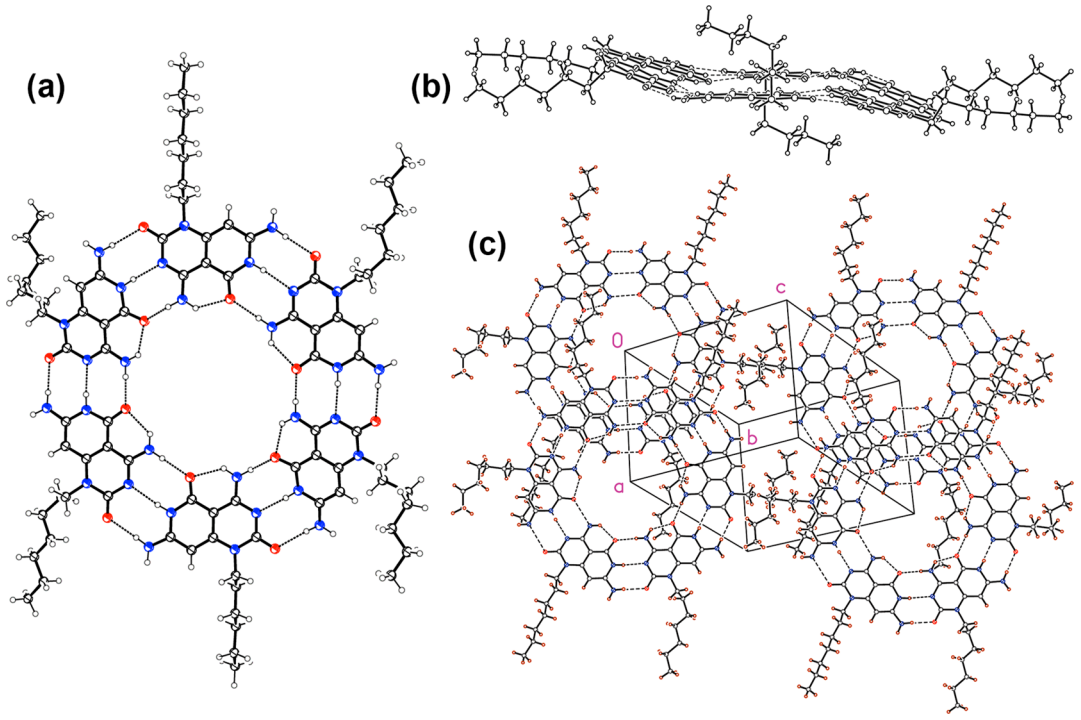

Figure 1. (a) Top view of X-ray crystal structure of $(\mathbf{3a})_6$ showing the hydrogen bonding array. (b) Side view showing the undulation of the central supermacrocyclic ring. (c) Portion of the stacking motif of the $(\mathbf{3a})_6$ hexamers. Solvent molecules are omitted for clarity.

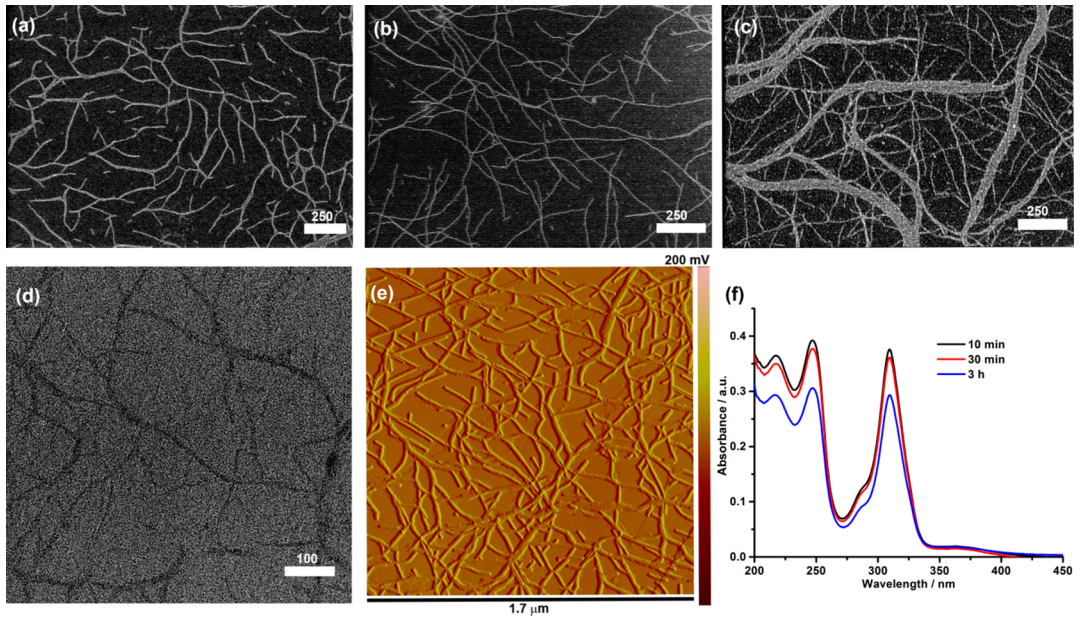

Figure 2. SEM images of **3b** (2.4×10^{-4} M) in cyclohexane at (a) 10 min (b) 2 days, and (c) 12 days. (d) TEM and (e) AFM images of **3b** in cyclohexane (2.4×10^{-4} M) at 10 min and 2 days, respectively. (f) Time-dependent UV−visible spectra of **3b** in cyclohexane (2.4×10^{-5} M). Scale bars are given in nm.

dependent spectra (Figure 2f and Figure S5 (Supporting Information)), **3b** presented three maxima at 217, 247, and 310 nm. When the self-assembly was monitored over a period of 3 h, a hypochromic effect was observed, which is indicative of increased $\pi-\pi$ stacking interactions and the growth of the nanotubes.[14] A 10-fold dilution of the stock solution of **3b** to a concentration of 2.4×10^{-5} M did not alter the UV−visible spectra, suggesting that the RNTs are kinetically stable (data not shown).

CONCLUSION

We have described a synthetic approach to the preparation of G∧C nucleobase hybrids in the form of self-assembling, N1-substituted pyrido[4,3-*d*]pyrimidines which are only 6 steps from the commercially available malononitrile dimer, representing a significant improvement on our earlier 10−12-step syntheses. In this demonstration work, pivotal intermediate **7** was simply alkylated to provide material for crystallographic and microscopic analysis, but it has the potential to act as a

dx.doi.org/10.1021/jo4019792 | J. Org. Chem. 2013, 78, 11421−11426

vehicle for the co-organization of a variety of species in a hexagonal array by substitution with functional tailgroups. The N1-heptyl pyrido[4,3-*d*]pyrimidine **3a** could be crystallized, and an X-ray structure determination confirmed the presence of the $(\mathbf{3a})_6$ hexamer assembled by 18 hydrogen bonds. The supermacrocyclic ring encloses a ca. 10.5 Å cavity, although there is only partial overlap of the hexamers in the crystal and no channels in the structure. The N1-hexadecyl pyrido[4,3-*d*]pyrimidine **3b**, on the other hand, undergoes rapid self-assembly into RNTs in cyclohexane. AFM, SEM, and TEM imaging studies showed the formation of 1D nanostructures with cross sections in excellent agreement with the modeled outer diameter of the RNTs.

EXPERIMENTAL SECTION

X-ray Crystal Structure Determination of 3a. Clusters of triangular plates were obtained from DMSO solution. The crystal selected for data collection was a colorless needle of dimensions 0.010 × 0.020 × 0.220 mm. The crystal was mounted in a 90 K nitrogen cold stream on the goniometer head of a diffractometer equipped with a CCD detector. Data were collected with the use of synchrotron radiation (λ = 0.8856 Å) at Beamline 11.3.1 at the Advanced Light Source, Lawrence Berkeley Laboratory. The structure was solved by a dual-space method (SHELXT) and refined by full-matrix least squares on F^2 (SHELXL-2012).[15] One of the three DMSO molecules is disordered over two orientations. The relative occupancies are 0.874(3)/0.126(3). The minor orientation was refined as a rigid group. In the minor orientation, isotropic displacement parameters were employed; in addition, one of the carbon atoms was assigned a fixed isotropic parameter of 0.08 in order to achieve convergence. All other non-hydrogen atoms were refined with anisotropic displacement parameters. R1 (7038 reflections with $I > 2\sigma(I)$) = 0.0748, wR2 (all 9948 data) = 0.231, 690 parameters, 0 restraints.

Sample Preparation for TEM, SEM, and AFM Imaging Studies. The G∧C base **3b** was dissolved in cyclohexane (0.5 mg/mL) by sonicating for 5 min at room temperature. The samples were aged at room temperature for the specified time period and then diluted to the stated concentration prior to imaging.

SEM samples were prepared by depositing the solutions on carbon-coated 400 mesh copper grids and blotting after 10 s. All samples were air-dried and heated on a hot plate under vacuum for 10 min prior to imaging to remove any residual solvents. SEM and STEM images were obtained without negative staining at a 10−30 kV accelerating voltage, 20 μA, and a working distance of 5−8 mm on a high-resolution cold field emission SEM and ultrahigh-resolution cold field emission SEM.

TEM samples were prepared by depositing a droplet of the RNT solution on a carbon-coated 400 mesh copper grid, followed by blotting after 10 s. The samples were then stained by depositing one droplet of uranyl acetate (2% in water or acetonitrile) for 120 s each. The grid was then blotted and dried in air with the use of a vacuum hot plate. TEM investigations were carried out on a 200 kV Schottky field emission TEM instrument equipped with an in-column Ω filter. Bright field TEM images were acquired using energy filtered zero loss beams (slit width 10 eV).

For the AFM measurements, clean HOPG (highly ordered pyrolytic graphite) substrates (1 × 1 cm^2) were prepared and the samples were deposited by spin coating at 3500 rpm for 30 s. Sample surfaces were observed using a Digital Instruments/Veeco Instruments MultiMode Nanoscope IV AFM equipped with an E scanner. For obtaining optimized height profiles, silicon cantilevers with low spring constants of 4.5 N/m were used in tapping mode (TM-AFM). To obtain a clear image, low scan rates (0.5−1 Hz) and amplitude set points (1 V) were chosen during the measurements.

Modeling. Monte Carlo Multiple Minimum (MCMM) procedure was carried out to search for the C16 side chain conformations that are in agreement with TEM and AFM measurements (Figure S6 (Supporting Information)).[16] The motif was modeled using the OPLS2005 force field, and the geometry optimization was carried out in the gas phase. Among the 270 conformations generated by the 1000 steps of the MCMM search, we selected one conformation (Figure S7a (Supporting Information)), which can form the six-membered rosette ring (Figure S7b (Supporting Information)) having a diameter of 4.4 nm, in agreement with the AFM and TEM measurements.

The association of **3** was modeled on that of 4,7-diamino-1-methylpyrido[4,3-*d*]pyrimidine-2,5(1*H*,6*H*)-dione. Calculations were performed at the density functional B3LYP/6-31G** level of theory using the Gaussian09 program. Default methods and SCF convergence criteria were applied. Solution geometries and energies were computed using the self-consistent isodensity polarized continuum model (SCI-PCM)[17] as implemented in Gaussian09.

4,6-Diamino-2-bromonicotinonitrile (5). A modification of the method of Carboni et al. was used:[18] a solution of the malononitrile dimer **4** (1.00 g, 7.57 mmol) in 33% HBr/HOAc (10 mL) was stirred overnight and then poured into a mixture of saturated aqueous $NaHCO_3$ (90 mL) and ethyl acetate (3 mL). The resulting precipitate was filtered and washed with water to give **5** as an off-white solid (1.27 g, 79%): ^{1}H NMR (400 MHz, DMSO-d_6) δ 6.64 (s, 2H), 6.51 (s, 2H), 5.57 (s, 1H); ^{13}C NMR (100 MHz, DMSO-d_6) δ 161.1, 157.9, 144.2, 117.5, 86.9, 85.8.

***N*-(4-Amino-6-bromo-5-cyanopyridin-2-yl)acetamide (6).** A modification of the method of Szczepankiewicz et al. was used:[19] to a solution of **5** (10.1 g, 47.3 mmol) in dry pyridine (100 mL) was slowly added acetyl chloride (9.0 mL, 9.9 g, 0.13 mol) at 0 °C. The mixture was stirred at 0 °C for 45 min, and then cold water (500 mL) was added and the resulting precipitate was filtered and washed with cold water to give **6** as a light brown solid (9.76 g, 80%): ^{1}H NMR (400 MHz, DMSO-d_6) δ 10.62 (s, 1H), 7.48 (s, 1H), 7.28 (s, 2H), 2.0 (s, 3H); ^{13}C NMR (100 MHz, DMSO-d_6) δ 170.4,160.0, 153.3, 143.4, 116.5, 95.8, 90.8, 24.6.

4,7-Diamino-5-methoxypyrido[4,3-*d*]pyrimidin-2(1*H*)-one (7). To a solution of **6** (6.41 g, 25.1 mmol) in dry CH_2Cl_2 (1.2 L) was added trichloroacetyl isocyanate (6.0 mL, 9.5 g, 50 mmol), and the mixture was stirred at room temperature for 2 days. The reaction was quenched with water (90 mL) followed by addition of saturated aqueous sodium bicarbonate (600 mL). The layers were separated, and the aqueous phase was washed (×5) with a 5% isopropyl alcohol/DCM mixture. The organic fractions were combined and dried over $MgSO_4$, and the solvent was evaporated. The resulting solid was dissolved in dry methanol (480 mL), and a solution of sodium methoxide prepared from sodium (5.09 g, 221 mmol) and methanol (725 mL) was added. The mixture was stirred at room temperature for 1 h and then heated at reflux overnight. The solvent was evaporated, acetic acid (35 mL) was added, and the resulting precipitate was filtered and washed with water to give **7** as an off-white solid (3.78 g, 73%): mp >320 °C dec; ^{1}H NMR (400 MHz, DMSO-d_6) δ 11.19 (br s, 1H), 9.02 (br s, 1H), 8.09 (s, 1H), 7.06 (s, 2H), 5.73 (s, 1H), 3.91 (s, 3H); ^{13}C NMR (100 MHz, DMSO-d_6) δ 162.6, 161.7, 159.9, 153.4, 151.3, 83.6, 83.1, 54.4; ESI-HRMS calcd for $C_8H_9N_5O_2$ [M + H] 208.0829, found 208.0826.

4,7-Diamino-1-heptyl-5-methoxypyrido[4,3-*d*]pyrimidin-2(1*H*)-one (8a). To a solution of **7** (0.200 g, 0.965 mmol) in dry DMF (40 mL) was added 60% sodium hydride (57.9 mg, 1.45 mmol), and the mixture was stirred at room temperature for 15 min. 1-Bromoheptane (0.310 mL, 0.345 g, 1.93 mmol) and sodium iodide (20.0 mg, 0.133 mmol) were added, and the mixture was stirred for 4 days. The reaction was quenched by the addition of MeOH (20 mL), and the solvent was evaporated. The residue was chromatographed on silica gel (10% methanol/DCM) to give **8a** (0.221 g, 75%) as an off-white solid: mp 145−147 °C; ^{1}H NMR (400 MHz, DMSO-d_6) δ 8.00 (br s, 1H), 7.56 (s, 1H), 6.83 (s, 2H), 5.78 (s, 1H), 3.92 (s, 3H), 3.81−3.75 (m, 2H), 1.54−1.47 (m, 2H), 1.29−1.19 (m, 8H), 0.82 (t, J = 6.9 Hz, 3H); ^{13}C NMR (100 MHz, DMSO-d_6) δ 162.6, 161.3, 160.7, 154.7, 151.6, 84.9, 82.4, 54.3, 43.2, 31.7, 28.9, 27.0, 26.8, 22.5, 14.4; ESI-HRMS calcd for $C_{15}H_{23}N_5O_2$ [M + H] 306.1925, found 306.1928.

4,7-Diamino-1-heptylpyrido[4,3-*d*]pyrimidine-2,5(1*H*,6*H*)-dione (3a). To a solution of **8a** (0.480 g, 1.57 mmol) in dry acetonitrile (175 mL) were added sodium iodide (1.50 g, 9.99 mmol) and chlorotrimethylsilane (0.836 mL, 0.715 g, 6.59 mmol). The

dx.doi.org/10.1021/jo4019792 | J. Org. Chem. 2013, 78, 11421−11426

reaction flask was protected from light and the mixture was heated at reflux for 2 h. The mixture was poured into pH 7 aqueous phosphate buffer (0.4 M, 150 mL). The resulting precipitate was filtered, washed with EtOAc, and recrystallized from DMSO to give **3a** as an off-white solid (0.349 g, 76%): mp >325 °C dec; ^{1}H NMR (400 MHz, DMSO-d_6/3 drops of *d*-TFA) δ 11.92 (s, 1H), 9.54 (s, 1H), 8.78 (s, 1H), 7.8 (br s, 2H), 5.54 (s, 1H), 3.78−3.70 (m, 2H), 1.57−1.48 (m, 2H), 1.33−1.15 (m, 8H), 0.82 (t, J = 6.0 Hz, 3H); ^{13}C NMR (100 MHz, DMSO-d_6) δ 162.0, 157.0, 156.3, 152.4, 148.0, 83.1, 77.7, 43.6, 31.6, 28.8, 26.7, 26.5, 22.4,14.3; ESI-HRMS calcd for $C_{14}H_{21}N_5O_2$ [M + H] 292.1768, found 292.1771.

4,7-Diamino-1-hexadecyl-5-methoxypyrido[4,3-*d*]-pyrimidin-2(1*H*)-one (8b). To a solution of **7** (0.200 g, 0.965 mmol) in dry DMF (40 mL) was added 60% sodium hydride (57.9 mg, 1.45 mmol), and the mixture was stirred at room temperature for 15 min. 1-Bromohexadecane (0.59 mL, 0.59 g, 1.9 mmol) and sodium iodide (20.0 mg, 0.133 mmol) were added, and the mixture was stirred for 4 days. The reaction was quenched by the addition of MeOH (20 mL), and the solvent was evaporated. The residue was chromatographed on silica gel (10% methanol/DCM) to give **8b** (0.266 g, 64%) as an off-white solid: mp 128−130 °C; ^{1}H NMR (400 MHz, DMSO-d_6) δ 8.02 (br s, 1H), 7.58 (br s, 1H), 6.84 (s, 2H), 5.79 (s, 1H), 3.92 (s, 3H), 3.81−3.74 (m, 2H), 1.54−1.47 (m, 2H), 1.29−1.16 (m, 26H), 0.81 (t, J = 7.0 Hz, 3H); ^{13}C NMR (100 MHz, DMSO-d_6) δ 162.6, 161.4, 160.6, 154.6, 151.6, 84.8, 82.5, 54.3, 43.2, 31.7, 29.52 (5C overlapped), 29.51, 29.48, 29.45, 29.3, 29.2, 27.0, 26.8, 22.5, 14.4; ESI-HRMS calcd for $C_{24}H_{41}N_5O_2$ [M + H] 432.3333, found 432.3330.

4,7-Diamino-1-hexadecylpyrido[4,3-*d*]pyrimidine-2,5-(1*H*,6*H*)-dione (3b). To a solution of **8b** (0.170 g, 0.393 mmol) in dry acetonitrile (60 mL) were added sodium iodide (0.438 g, 2.92 mmol) and chlorotrimethylsilane (0.245 mL, 0.209 g, 1.93 mmol). The reaction flask was protected from light and the mixture was heated at reflux for 2 h. The mixture was poured into pH 6.5 aqueous phosphate buffer (0.4 M, 50 mL). The resulting precipitate was filtered and washed with EtOAc and then with MeOH to give **3b** as an off-white solid (0.158 g, 96%): mp >305 °C dec; ^{1}H NMR (400 MHz, DMSO-d_6, 3 drops of *d*-TFA) δ 11.90 (s, 1H), 9.54 (s, 1H), 8.71 (s, 1H), 7.8 (br s, 2H), 5.54 (s, 1H), 3.79−3.71 (m, 2H), 1.57−1.48 (m, 2H), 1.30−1.13 (m, 26H), 0.84−0.76 (m, 3H); ^{13}C NMR (100 MHz, DMSO-d_6) δ 162.0, 156.9, 156.2, 152.4, 147.9, 83.1, 77.7, 43.6, 31.7, 29.5 (8C overlapped), 29.4, 29.2, 26.7, 26.6, 22.5, 14.3; ESI-HRMS calcd for $C_{23}H_{39}N_5O_2$ [M + H] 418.3177, found 418.3172.

■ ASSOCIATED CONTENT

Supporting Information

Text, figures, tables, and a CIF file giving the full citation for Gaussian09, Cartesian coordinates and energies for all calculations used in this work, experimental details for the X-ray crystal structure determination of **3a**, numbering scheme for the X-ray crystal structure determination of **3a**, crystallographic data **3a**, experimental details of the imaging of **3b**, UV−vis studies of the aggregation of **3b**, modeling of the aggregation of **3b**, and ^{1}H and ^{13}C NMR data for compounds **3a**,**3b**, **5**−**7**, and **8a**,**b**. This material is available free of charge via the Internet at http://pubs.acs.org.

■ AUTHOR INFORMATION

Corresponding Authors

*E-mail for M.M.: mjmascal@ucdavis.edu.
*E-mail for H.F.: h.fenniri@neu.edu.

Notes

The authors declare no competing financial interest.

■ ACKNOWLEDGMENTS

We thank the Advanced Light Source, Beamline 11.3.1, Lawrence Berkeley Laboratory, for support. The Advanced Light Source is supported by the Director, Office of Science, Office of Basic Energy Sciences, of the U.S. Department of Energy under Contract No. DE-AC02-05CH11231. Support from the Natural Science and Engineering Research Council of Canada, the National Research Council of Canada, the University of Alberta, and Northeastern University are gratefully acknowledged.

■ REFERENCES

(1) (a) Bong, D. T.; Clark, T. D.; Granja, J. R.; Ghadiri, M. R. *Angew. Chem., Int. Ed.* **2001**, *40*, 988. (b) Gong, B.; Shao, Z. *Acc. Chem. Res.* **2013**, DOI: 10.1021/ar400030e. (c) Garcia-Fandino, R.; Amorin, M.; Granja, J. R. In *Supramolecular Chemistry: From Molecules to Nanomaterials;* Gale, P. A.; Steed, J. W., Eds.; Wiley: Chichester, U.K., 2012; Vol. *5*, pp 2149.

(2) Frontera, A.; Gamez, P.; Mascal, M.; Mooibroek, T. J.; Reedijk, J. *Angew. Chem., Int. Ed.* **2011**, *50*, 9564.

(3) Metrangolo, P.; Meyer, F.; Pilati, T.; Resnati, G.; Terraneo, G. *Angew. Chem., Int. Ed.* **2008**, *47*, 6114.

(4) (a) Mascal, M.; Hext, N. M.; Warmuth, R.; Moore, M. H.; Turkenburg, J. P. *Angew. Chem., Int. Ed. Engl.* **1996**, *35*, 2204. (b) Marsh, A.; Silvestri, M.; Lehn, J.-M. *Chem. Commun.* **1996**, 1527. (c) Kolotuchin, S. V.; Zimmerman, S. C. *J. Am. Chem. Soc.* **1998**, *120*, 9092. (d) Mathivanan, P.; Vidale, K. L.; Sherman, D. M.; Hallenga, K.; Wood, K. V.; Stowell, J. G. *J. Am. Chem. Soc.* **2001**, *123*, 3854.

(5) (a) Mascal, M.; Warmuth, R.; Arnall-Culliford, J. R.; Moore, M. H.; Turkenburg, J. P. *J. Org. Chem.* **1999**, *64*, 8479. (b) Beingessner, R.; Deng, B.-L.; Fanwick, P. E.; Fenniri, H. *J. Org. Chem.* **2008**, *73*, 931. (c) Tikhomirov, G.; Oderinde, M.; Makeiff, D.; Mansouri, A.; Weibing, L.; Heirtzler, F. R.; Kwok, D. Y.; Fenniri, H. *J. Org. Chem.* **2008**, *73*, 4248. (d) Fenniri, H.; Deng, B.-L.; Ribbe, A. E. *J. Am. Chem. Soc.* **2002**, *124*, 11064.

(6) Computational modeling was carried out at the density functional B3LYP/6-31G(d,p) level of theory using the Gaussian09 program (Gaussian, Inc., Wallingford, CT, 2004, 2009; full Gaussian 09 reference in Supporting Information). Default methods and SCF convergence criteria were applied.

(7) Mascal, M.; Farmer, S. C.; Arnall-Culliford, J. R. *J. Org. Chem.* **2006**, *71*, 8146.

(8) Supramolecular Macrocycle Synthesis by H-bonding Assembly (review): Ballester, P.; de Mendoza, J. In *Modern Supramolecular Chemistry*; Diederich, F., Stang, P. J., Tykwinski, R. R., Eds.; Wiley-VCH: Weinheim, Germany, 2008 pp 69.

(9) Lipps, H. J.; Rhodes, D. *Trends Cell Biol.* **2009**, *19*, 414.

(10) (a) Theobald, J. A.; Oxtoby, N. S.; Phillips, M. A.; Champness, N. R.; Beton, P. H. *Nature* **2003**, *424*, 1029. (b) Räisänen, M. T.; Slater (née Phillips), A. G.; Champness, N. R.; Buck, M. *Chem. Sci.* **2012**, *3*, 84.

(11) (a) Moralez, J. G.; Raez, J.; Yamazaki, T.; Motkuri, R. K.; Kovalenko, A.; Fenniri, H. *J. Am. Chem. Soc.* **2005**, *127*, 8307. (b) Johnson, R. S.; Yamazaki, T.; Kovalenko, A.; Fenniri, H. *J. Am. Chem. Soc.* **2007**, *129*, 5735. (c) Borzsonyi, G.; Beingessner, R. L.; Yamazaki, T.; Cho, J.-Y.; Myles, A. J.; Malac, M.; Egerton, R.; Kawasaki, M.; Ishizuka, K.; Kovalenko, A.; Fenniri, H. *J. Am. Chem. Soc.* **2010**, *132*, 15136.

(12) Since the hexamer crystallizes out of DMSO, a reviewer suggested we recalculate the H-bonding energy of the assembly in this solvent. Whereas the gas-phase association energy for each pairing was 29.7 kcal mol^{-1}, in DMSO this value decreases to 18.4 kcal mol^{-1}, which amounts to a 40% reduction. Although the pairing is less effective in solvent, there is still ample driving force to assemble the hexamer.

(13) (a) Cho, J.-Y.; Fenniri, H. *Imaging Microsc.* **2010**, *4*, 33. (b) Bustamante, C.; Vesenka, J.; Tang, C. L.; Rees, W.; Guthold, M.; Keller, R. *Biochemistry* **1992**, *31*, 22.

(14) A hypochromic effect is commonly observed in nucleic acid. Upon self-assembly and formation of a double helix, the two maxima in the UV region undergo a hypochromic shift. When the double helix is melted, the extinction coefficient increases to its original (molecular)

state, resulting in a hyperchromic effect. This phenomenon is used to investigate the cooperative nature of the self-assembly process in nucleic acids. We use the same strategy to establish the cooperative nature of RNT self-assembly.[4d]

(15) Sheldrick, G. M. *SHELXL-2012*; University of Göttingen, Göttingen, Germany, 2012.

(16) *MacroModel, version 9.9*; Schrödinger, LLC, New York, 2011.

(17) Foresman, J. B.; Keith, T. A.; Wiberg, K. B.; Snoonian, J.; Frisch, M. J. *J. Phys. Chem.* **1996**, *100*, 16098.

(18) Carboni, R. A.; Coffman, D. D.; Howard, E. G. *J. Am. Chem. Soc.* **1958**, *80*, 2838.

(19) Szczepankiewicz, B. G.; Kosogof, C.; Nelson, L. T. J.; Liu, G.; Liu, B.; Zhao, H.; Serby, M. D.; Xin, Z.; Liu, M.; Gum, R. J.; Haasch, D. L.; Wang, S.; Clampit, J. E.; Johnson, E. F.; Lubben, T. H.; Stashko, M. A.; Olejniczak, E. T.; Sun, C.; Dorwin, S. A.; Haskins, K.; Abad-Zapatero, C.; Fry, E. H.; Hutchins, C. W.; Sham, H. L.; Rondinone, C. M.; Trevillyan, J. M. *J. Med. Chem.* **2006**, *49*, 3563.